ELSEVIER

Journal of Nuclear Materials 241–243 (1997) 268–272

journal of nuclear materials

2D modelling of radiating divertor regime for ITER

A. Kukushkin [a,*], H.D. Pacher [c], M. Baelmans [d], D. Coster [b], G. Janeschitz [a], D. Reiter [d], R. Schneider [b]

[a] *ITER JCT, Garching JWS, Boltzmannstr. 2, 85748 Garching, Germany*
[b] *Max-Planck Institut für Plasmaphysik, Garching, Germany*
[c] *The NET Team, Garching, Germany*
[d] *Institut für Plasmaphysik, FZ Jülich, Germany*

Abstract

A modelling study of the ITER divertor is done using the B2-Eirene code package with full multi-species impurity treatment and volumetric recombination of deuterium ions. A 'virtual target regime' is identified, for which strong recombination and ionization form a double layer which acts like a target surface inside the divertor plasma. The power loads, erosion, and helium removal seem to be within the acceptable range for the ITER design, making this regime, together with operational points close to it, a reasonable starting point for the optimization of the ITER divertor.

Keywords: ITER; Divertor plasma; 2D model

1. Modelling setup

The B2-EIRENE code [1,2] is used to investigate a radiating divertor regime for ITER. The divertor geometry is that of the ITER EDA design [3] with vertical target outboard and semi-transparent structures in the private flux region ('wings') protected by a dome near the X-point. The plasma is deuterium with an admixture of helium and varying levels of neon. Volume recombination of deuterium is included, and full multi-fluid treatment of impurity transport is employed in the code.

We specify an input power of 200 MW and constant densities of D^+, He^{++}, and Ne^{10+} as the boundary conditions at the core, with the helium density always 10% that of deuterium, and the neon fraction as the principal input parameter in this study. The densities of lower impurity charge states are set to zero at this boundary (justified by the high temperature there). At the targets, we assume 100% recycling for all species and we apply the usual sheath conditions with $M \geq 1$. The cross-field transport coefficients are constant; $\chi_\perp = 1$ m^2/s, $D_\perp = 0.3$ m^2/s for all plasma species in the main study. We also assume that some pumping is done from the private flux region (PFR), specifying an albedo of 95% for the neutrals at the duct entrance and—only to stabilize the transition to detachment—50% recycling for the plasma ions diffusing into the PFR across the magnetic field. We have performed most scans as a function of neon density. Several cases with different values of $D_\perp$, $\chi_\perp$, and plasma density are also calculated.

2. Transition to detachment

The imposed increase in neon density is accompanied by an increase of the radiated power and a decrease of the power coming to the targets (Fig. 1). Increasing radiative losses, although not proportional to the neon density, reduce the power to the divertors and facilitate a partial detachment of the plasma from the divertor targets, for both inner and outer divertors, Fig. 2. The particle flux reaching the targets also goes down together with the plasma pressure in the divertors, in accordance with the typical picture of plasma detachment. The value $Z_{\text{eff}} \cong 2$ at the core after detachment is somewhat higher than that

* Corresponding author. Tel.: +49-89 3299 4122; fax: +49-89 3299 4110; e-mail: ank@sat.ipp-garching.mpg.de.

PII S0022-3115(96)00512-0

accepted for ITER [4], but can probably be reduced by further optimization of the gas puffing and impurity seeding scheme and by inclusion of intrinsic impurities (Be, C). The impurity level necessary to reach detachment is here significantly higher than for a fixed impurity fraction model, because the thermal force and cross-field transport drive impurities to the very edge of the scrape-off layer (SOL) [5], out of the hot zone, reducing their radiation efficiency. It is worth noting that the experimentally observed trend of equilibration of the power coming to the inner and outer divertor is clearly seen here (but we do not include drifts in our calculations).

3. Virtual target

Analysis of the simulations shows that the sharp increase of the radiated power in the course of the detachment, Fig. 1, is to be attributed to the line radiation from neutrals, mostly hydrogen, rather than to radiation from impurity ions, see Fig. 3, and this seems to be consistent with the Alcator-Cmod experiment [6]. While the ion flux to the targets and wall decreases by a factor of 2, the neutral-related radiation increases, yielding around 75 eV of radiated power per ion eventually recombining at the surface. At first glance, this appears inconsistent with high-density, low-temperature divertor plasma for which the radiation per ionization event should be small [7]. The picture becomes clear when volumetric recombination, included in the calculations, is evaluated. Fig. 4 shows the net source of deuterium ions integrated over the volume and that due to recombination (negative). One can see that the absolute value of the recombination source becomes 5 times greater than the net source, indicating strong recycling in the volume. The neutrals born in recombination become ionized, the ions recombine, and so on, on average 5 times before the ion reaches a material surface. For the typical range of plasma density ($\approx 10^{21}$ m^{-3}) and temperature (≈ 1 eV) in the recombination zone, the radiation loss per recombination event is around 10 eV [8], and the remaining 5 eV are radiated during subsequent ionization. For such recycling in the volume to be efficient, there must be a strong gradient of plasma temperature and/or density. Indeed, the temperature ranges for efficient ionization and recombination are > 5 eV and < 2 eV, respectively, and neutrals must be able to reach the higher temperature region before escaping from the plasma. Fig. 5 shows that a double layer configuration of adjacent strong ionization/recombination regions constituting a sharp ionization front is formed, acting like a target and ensuring efficient recycling of hydrogen isotopes far from the material surfaces (unlike Ref. [9] for which the recombination occurred close to the target). The profiles of the plasma parameters such as temperature, density, and radiation intensity are aligned with this front, in analogy with a real target. Moreover, the plasma flow becomes supersonic beyond the front, satisfying the Bohm criterion $M \geq 1$ at the virtual target, Fig. 6. This could create a shock which causes a density increase upstream of the front, thus facilitating the formation of the necessary gradients. It is worth noting that the qualitative picture looks superficially similar to that of Ref. [10], but the physical mechanisms are indeed quite different.

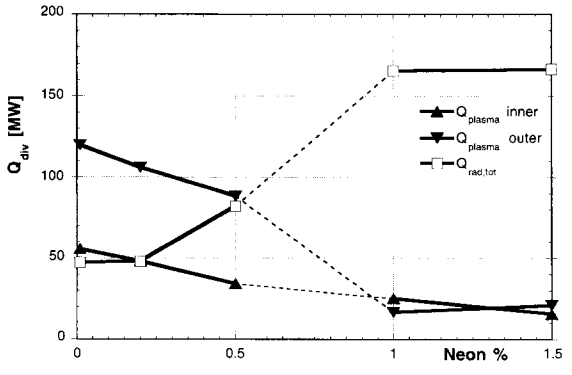

Fig. 1. Total power to targets including plasma + neutrals (conduction, ion convection, surface recombination, neutral convection, molecular dissociation) and radiation (neutral, ion, Bremsstrahlung).

4. Target and wall loading

One of the primary quantities for divertor design is the peak power load on the target. The variation of this peak power load for both targets with neon concentration is shown in Fig. 7. As the neon level is increased from 0.5% to 1% and volumetric recombination becomes dominant, the peak load on the outer target, which is more severely loaded, drops from 11 to 1.5 MW/m^2. The profiles of power loading of the targets for these two cases are given in Fig. 8. Despite the drastic increase of total radiation power, the radiation power coming to the target stays below 0.8 MW/m^2, because the radiation source is now spread along the virtual target. One can see a qualitative difference between the profiles for the two regimes, which may imply a bifurcation. A minor variation of the cross-field transport ($\chi_\perp = 0.6$ m^2/s, $D_\perp = 0.2$ m^2/s in the 0.5% Ne case) does not change the picture—although the peak before detachment becomes higher, around 14 MW/m^2.

The radiation power load can reach almost 3 MW/m^2 for the structures located in the PFR ('wings' and dome), 1 MW/m^2 for the baffles, and 0.2 MW/m^2 for the first wall in the main chamber. The power delivered by charge-exchange neutrals to the walls remains low, but the neutral particle flux to the dome can be significant, around $5 \cdot 10^{22}$ m^{-2} s^{-1}. Although the average neutral energy is below 3 eV, high-energy tails might cause a considerable

sputtering of a low-Z material such as Be or C there. It should be noted that the plasma fuelling in our model is artificial; once realistic gas puffing somewhere in the main chamber is taken into account, the local neutral fluxes onto the first wall and corresponding erosion can become significant.

5. Helium removal

The issue of helium removal is also critical for ITER. Helium ions, like other impurities, are subject to the thermal force in the SOL. This force impedes the helium flow to the target in the hot zone adjacent to the separatrix,

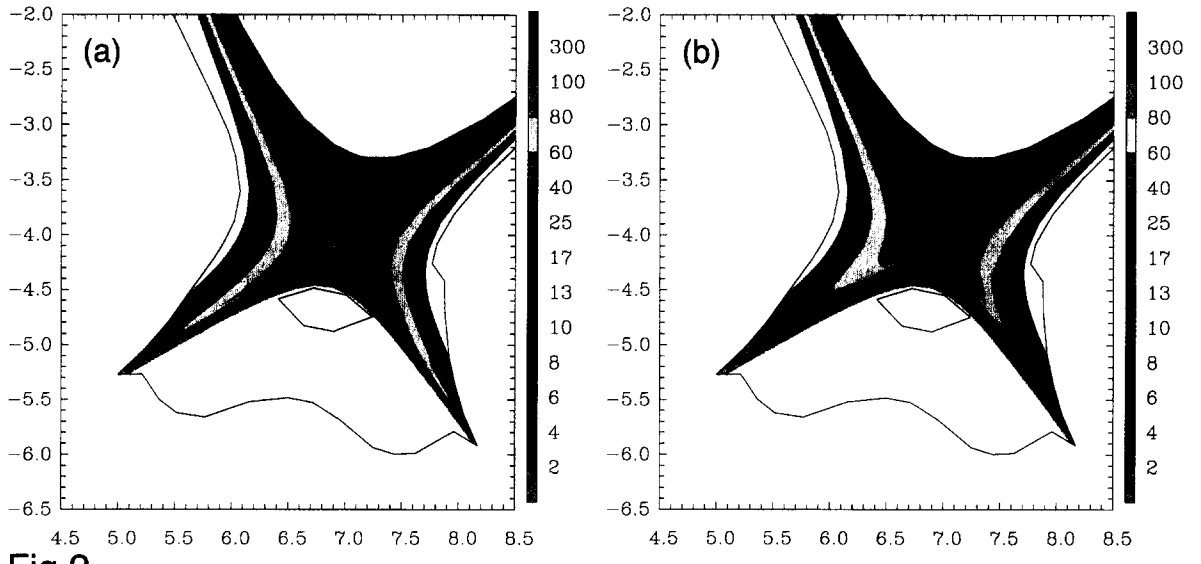

Fig.2

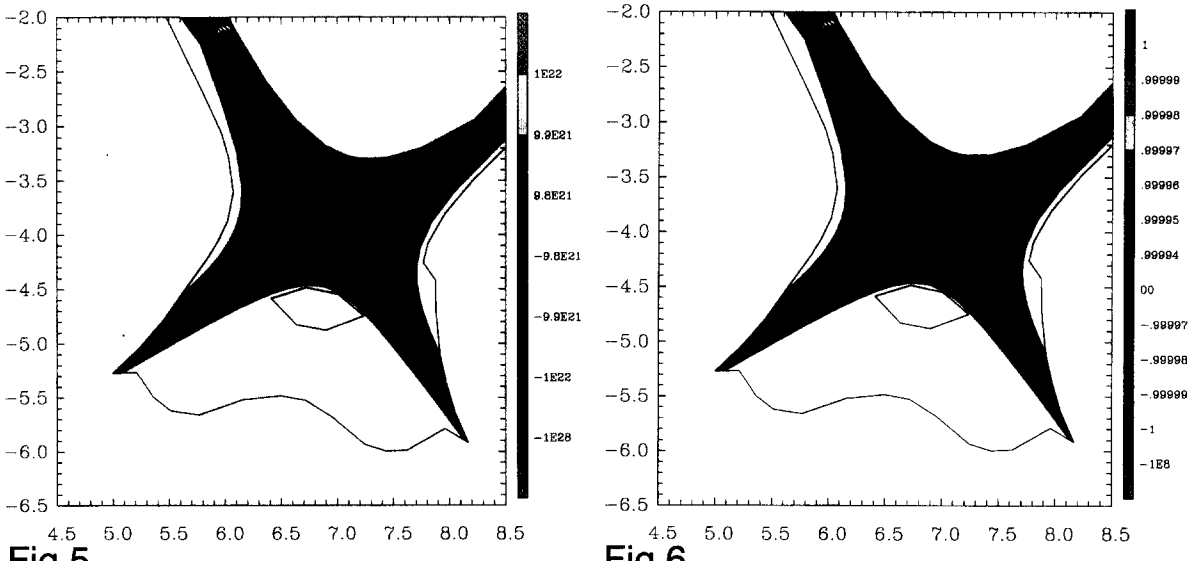

Fig.5 Fig.6

Fig. 2. Profiles of electron temperature for (a) 0.5% Ne and (b) 1% Ne.

Fig. 5. Ionization/recombination front in the divertor plasma. Regions for which the net particle source is strongly positive are shown yellow (lightest), those with strong recombination are shown magenta (darkest).

Fig. 6. Supersonic transition at the virtual target and flow pattern. Regions of supersonic flow are shown magenta and red (darkest) inboard and outboard, respectively, those having subsonic flow directed from the outer to the inner divertor (negative values) are shown turquoise (lightest). The opposite direction is green (darker).

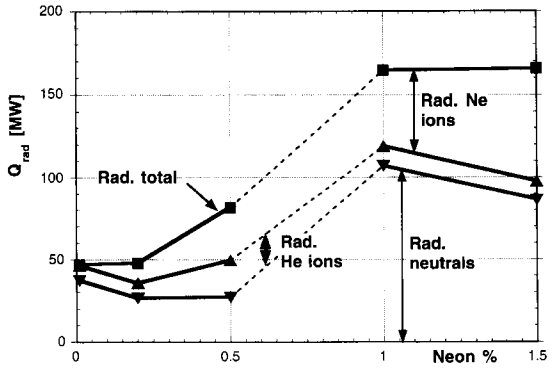

Fig. 3. Contributions of radiation from different sources (neutrals, He ions, Ne ions) to the total power radiated in the SOL and divertor versus neon fraction. Bremsstrahlung in the SOL is negligible.

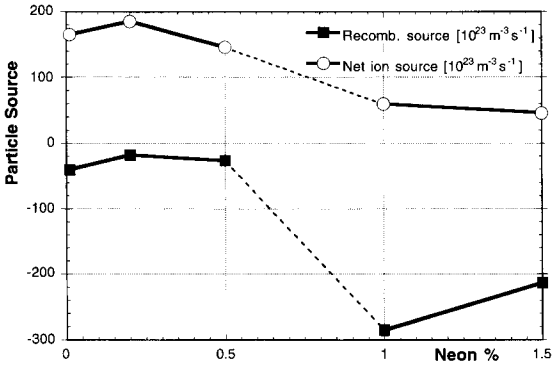

Fig. 4. Total net ion source and total ion source from recombination versus neon fraction.

making the helium diffuse outward and recombine at the outboard part of the target. Given the present ITER geometry, for which pumping is from the PFR, the helium atoms

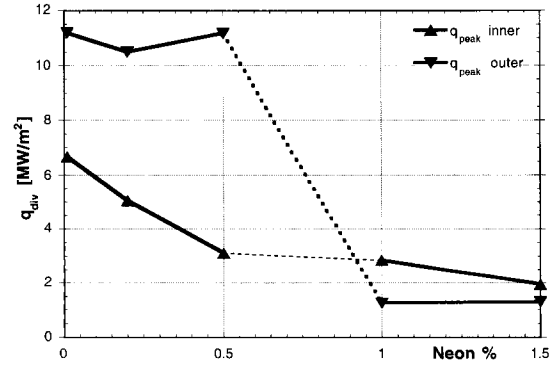

Fig. 7. Peak power load on the targets from plasma and neutrals (conduction, ion convection, surface recombination, neutral convection, molecular dissociation) and radiation (neutral, ion, bremsstrahlung), versus neon fraction.

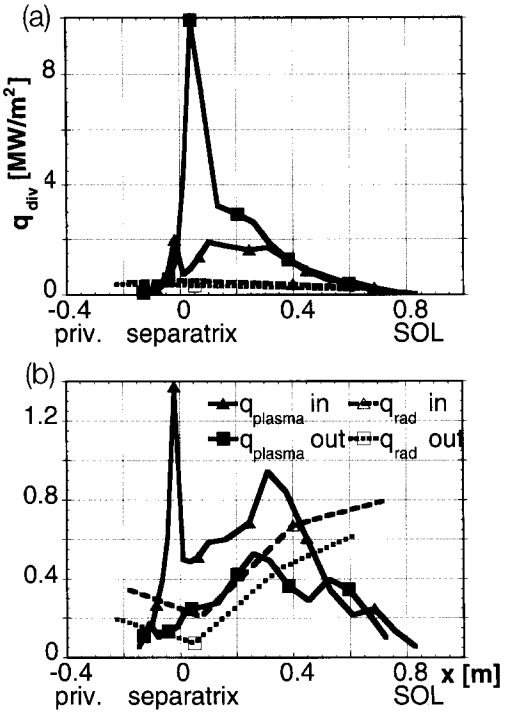

Fig. 8. Profiles of power load on the divertor targets (particles and radiation) for (a) 0.5% Ne and (b) 1% Ne.

have to traverse the divertor plasma to reach the pumping duct, and this can make their removal quite inefficient [5]. The efficiency of helium exhaust can be discussed in terms of the helium enrichment factor η, which is the ratio of relative helium concentration in the pumped-out gas to that in the core plasma, and of the neutral pressure in the

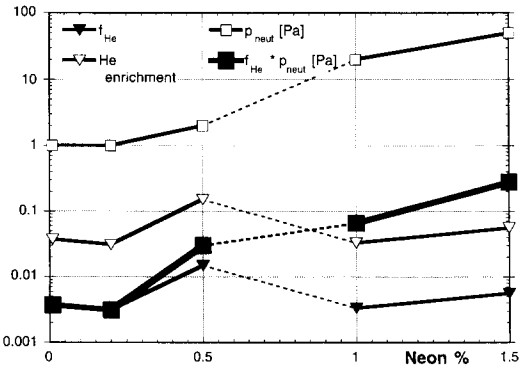

Fig. 9. Helium fraction, helium enrichment, deuterium neutral pressure, and helium 'partial pressure' (helium fraction times deuterium pressure) versus neon fraction. He fraction is helium flux over deuterium flux at the pump surface, He enrichment is this helium fraction over the ratio of helium and deuterium densities at the core, deuterium pressure is measured at the plasma edge in the private flux region.

pumping duct P_{neut}. Since the required helium exhaust rate is determined by the fusion power, these two parameters give the relation between the helium concentration in the core and the pumping speed. The variation of the reference parameters with neon concentration in the core is given in Fig. 9. Simple estimates show that the neutral gas in the PFR must be collisional, whereas our Monte-Carlo package used for the neutral transport calculations does not treat neutral–neutral collisions. Therefore the neutral pressure in the PFR (at the duct entrance) is estimated here to be equal to the average neutral pressure at the plasma boundary in the PFR. Whenever the helium pressure reaches 0.01 Pa at the entrance of the pump duct, the pumping system of ITER as designed presently can remove the necessary amount of helium to ensure steady-state operation. Our calculations indicate that this goal could be achieved, and that the helium exhaust conditions become more favorable with transition to the virtual target regime.

6. Discussion

The virtual target makes a small angle with the magnetic surfaces, causing gradients across the field to play a dominant role in the formation of the double layer. Therefore the cross-field transport of plasma becomes extremely important for this kind of operation, and this process is one of the less certain parts of our present knowledge. It seems however unlikely that the transport in the more turbulent divertor region is weaker than inside the separatrix.

Given the significance of radiation losses from hydrogen in the power balance of the virtual target regime, the issue of radiation transport through the dense cloud of gas becomes important. A simple estimate [11] gives a mean-free-path of the order of 1 mm for L_α radiation in the divertor. Probably, the geometry of the virtual target (elongated and thin) could alleviate the problem.

Inclusion of the light impurities (Be, C) in the model could probably enhance the radiation losses due to their higher emissivity at low temperature. This work is still to be done.

7. Conclusions

Modelling shows that a 'virtual target regime' might be feasible in the ITER divertor with vertical target plates. Strong ionization and recombination form a sharp front which acts like a target, ensuring efficient recycling of hydrogen isotopes in the volume, far from the material surfaces. Radiation accompanying the recombination–ionization process is the major mechanism of power dissipation. The profiles of plasma parameters are aligned with the virtual target, and the plasma flow becomes supersonic beyond the front.

This regime, together with operational points close to it, can be used as the starting point for the optimization of the ITER divertor. Operation in this regime would result in acceptable power loads, probably acceptable erosion, and acceptable conditions for helium removal.

Among the key issues requiring special attention are the following: studies of sensitivity of the solution to the model assumptions; assessment of transport of line radiation through the dense neutral gas; refinement of the atomic data on impurity radiation, ionization and recombination; insight into the cross-field transport of the edge plasma supported by model validation against the experimental data; optimization of gas puffing and impurity seeding; analysis of the effect of the divertor geometry.

Acknowledgements

This report has been prepared as an account of work performed under the Agreement among the European Atomic Energy Community, the Government of Japan, the Government of the Russian Federation, and the Government of the United States of America on Cooperation in the Engineering Design Activities for the International Thermonuclear Experimental Reactor (''ITER EDA Agreement'') under the auspices of the International Atomic Energy Agency (IAEA). The work of M.B. has been supported by EURATOM in the frame of its fellowship scheme.

References

[1] D. Reiter, H. Kever, G.H. Wolf et al., Plasma Phys. Controlled Fusion 33 (1991) 1579.
[2] R. Schneider, D. Reiter, H.-P. Zehrfeld et al. J. Nucl. Mater. 196–198 (1992) 810.
[3] R. Parker, these Proceedings, p. 1.
[4] G. Janeschitz et al., Plasma Phys. Controlled Fusion 37 (1995) A19.
[5] S.I. Krasheninnikov, A.S. Kukushkin and T.K. Soboleva, Nucl. Fusion 31 (1991) 1455.
[6] J. Goetz, C. Kurz, B. LaBombard, B. Lipschultz et al., Phys. Plasmas, 3 (1996) 1908.
[7] R.K. Janev, D. Post, W. Langer et al., J. Nucl. Mater. 121 (1984) 10.
[8] D. Reiter, private communication.
[9] M. Petravic, Phys. Plasmas 1 (1994) 2209.
[10] M.L. Watkins and P.-H. Rebut, Proc. 1992 Int. Conf. on Plasma Physics, Innsbruck, Austria, Vol. 11 (1992) p. 731.
[11] D. Post, J. Nucl. Mater. 220–222 (1995) 143.